Internal variability of the dynamically downscaled tropical cyclone activity over the western North Pacific by the IPRC Regional Climate Model

Chun-Chieh Wu[1], Ruifen Zhan[2], Yi Lu[1], and Yuqing Wang[3]

[1]Department of Atmospheric Sciences, National Taiwan Univeristy, Taipei, Taiwan

[2]Shanghai Typhoon Institute of China Meteorological Administration, Shanghai, China

[3]International Pacific Research Center and Department of Meteorology, University of Hawaii at Manoa, Honolulu, Hawaii

September 12, 2011 (Accepted)

(***Journal of Climate***)

Corresponding author address: Chun-Chieh Wu, Dept. of Atmospheric Sciences, National Taiwan University, No. 1, Sec. 4, Roosevelt Rd., Taipei 106, Taiwan.

E-mail: cwu@typhoon.as.ntu.edu.tw

ABSTRACT

As synoptic storms, tropical cyclones (TCs) are highly nonlinear systems resulting from multiple scale interactions. In particular, the formation/genesis of TCs involves complex nonlinear processes, exhibiting strong internal variability in climate model simulations. This study attempts to examine such internal variability of dynamically downscaled TCs over the western North Pacific (WNP) based on four simulations of 20 typhoon seasons (1982–2001) initialized on four successive days using the International Pacific Research Center (IPRC) Regional Climate Model (iRAM). The results show that on both seasonal and interannual timescales, the initial conditions significantly affect the downscaled TC activity, with the largest internal variability occurring in August on the seasonal timescale. The spreads between any of the individual simulations and the ensemble mean are comparable to and in some circumstances greater than the interannual variation of the observed TC frequency. The internal variability of the downscaled TC activity is found to be insensitive to the amplitude and the pattern of the initial perturbations. However, day-to-day model solutions are strongly affected by the internal variability. As a result, the development of nonlinear atmospheric instabilities significantly modulates the genesis and development of the TC-like vortices, leading to the large internal variability of the downscaled TC activity. In addition to the traditional initial value problem, criteria (in particular, threshold values) used in the TC detection contribute equally to the internal variability of the downscaled TCs in the simulations. Consistent with earlier studies, our results also show that the ensemble mean provides the better downscaled information on seasonal and interannual frequencies of TC genesis and occurrence.

1. Introduction

High-resolution regional climate models (RCMs) have been widely used for dynamical downscaling of seasonal climate prediction and future climate projection in the last decades since the first successful demonstrations of regional climate modeling by Dickinson et al. (1989) and Giorgi and Bates (1989). Given detailed representations of physical processes, and high spatial resolution that resolves complex topography, land-sea contrast, and land use, an RCM driven by large-scale forcing can generate realistic regional climate information. It not only retains most of the large-scale information that can be appropriately resolved by the reanalysis or the general circulation models (GCMs), but also provides fine-scale details that could not be generated by the coarse-resolution reanalysis or GCMs. RCMs have proven to be a powerful tool in the dynamical downscaling for climate change and seasonal climate prediction and in regional climate process studies (see a review by Wang et al. 2004).

An important application of RCMs is to dynamically downscale the tropical cyclone (TC) activity. A number of studies have examined the ability of RCMs to improve the skills of the GCM in simulating the seasonal TC activity (e.g., Walsh and Syktus 2003; Landman et al. 2005; Camargo et al. 2007; Feser and Storch 2008). These studies have shown that RCMs can produce more realistic seasonal TC activity than a coarse-resolution GCM although the simulated TC intensity is still weaker than that observed. RCMs have been successfully utilized to improve our understanding of the factors controlling TC activity as well (e.g., Nguyen and Walsh 2001; Knutson et al. 2007; Zhan et al. 2011a). For example, using the International Pacific Research Center (IPRC) regional atmospheric model driven by the reanalysis and the observed sea surface temperatures (SSTs), Zhan et al. (2011a) discussed

the impact of SST anomaly (SSTA) in the East Indian Ocean (EIO) on the TC frequency over the western North Pacific (WNP) and the involved physical mechanisms proposed by Zhan et al. (2011b). More studies have focused on the influence of global warming on future TC activity in different ocean basins using high-resolution RCMs driven by the output of GCMs (e.g., Nguyen and Walsh 2001; Walsh et al. 2004; Stowasser et al. 2007; Knutson et al. 2008). RCMs are shown to be able to obtain the quantitative projections of TC activity at higher resolutions than GCMs and with dedicated physics adapted to the basin of interest.

Similar to GCMs, RCMs are subject to different sources of errors/uncertainties: the parameterizations of physical processes, the initial conditions, the numerical algorithms, surface forcing, etc. Since RCMs are run over limited-area domains and are driven by time-dependent large-scale meteorological fields specified in a buffer area adjacent to the domain's lateral boundaries, RCMs have one additional source of error related to their lateral boundary conditions (LBCs) (Warner et al. 1997). Many efforts have been made to examine the influence of the LBCs on the uncertainty in RCM simulations (Seth and Giorgi 1998; Nutter et al. 2004; Wu et al. 2005; Nicolis 2007; Vanvyve et al. 2008). These studies generally suggested that the LBC is critical to skillful long-term regional climate simulations. Landman et al. (2005) investigated the impact of the RCM domain choice on the simulation of TCs over the southwestern Indian Ocean and suggested that careful consideration of domain choice and the location of the lateral boundaries are essential to the simulated seasonal TC activity.

Compared to the pronounced impact of the LBCs, small perturbations in the initial conditions do not appear to significantly change the RCM solution (Giorgi and Bi 2000;

Vannitsem and Chome 2005; Wu et al. 2005; Vanvyve et al. 2008). Some previous studies have suggested that the signal representing internal variability induced by initial conditions weakens with time and thus the confidence in the simulations increases with the duration of the simulation (Wu et al. 2005; Vanvyve et al. 2008). However, the model internal variability can be in some circumstances as large as or larger than the signal induced the external forcings (e.g., Weisse et al. 2000; Christensen et al. 2001). For example, Weisse et al (2000) found that the impact of the sea state–dependent roughness on the atmospheric circulation appeared to be hidden by the internal variability of the model when the internal variability was high. In addition, some studies revealed that the RCM internal variability depends heavily on synoptic events and variables (Christensen et al. 2001; Caya and Biner 2004; Alexandru et al. 2007). This is consistent with the findings of Giorgi and Bi (2000), who demonstrated that the day-to-day model solutions are affected by the internal variability although the domain-wide statistics are not. As synoptic storms, TCs are highly nonlinear systems, and their genesis involves strong multiscale interactions. Dynamical simulations of TC activity by an RCM are thus likely sensitive to small changes in the initial conditions, even if the RCM is constrained by the same LBCs. In this sense, the downscaled TC activity on seasonal time scale in an RCM may be subject to strong internal variability. Therefore, it is necessary to evaluate the uncertainty associated with internal variability when we dynamically downscale TC activity on seasonal time scale.

In this study, four simulations for 20 typhoon seasons (1982–2001) with varying initial (successive) dates are conducted to examine the internal variability of dynamically downscaled TCs over the WNP using the IPRC regional atmospheric model (iRAM). It

should be mentioned that four members are not enough to thoroughly address the internal variability issue. Therefore, this work can be regarded as a pilot study to demonstrate the importance of this issue and to promote further efforts toward improved understanding of the internal variability of the dynamically downscaled TC activity. Nevertheless, we will show that the 4-member ensemble can provide the better downscaled information on seasonal and interannual frequencies of TC genesis and occurrence than any individual member. The rest of the paper is organized as follows. Section 2 provides a brief description of the model, experimental design, the datasets, and the analysis methods. Section 3 evaluates the performance of the dynamically downscaled large-scale features and TC climatology from four ensemble simulations and the ensemble mean. The internal variability of the downscaled WNP TCs is presented in section 4. The sources of uncertainties are discussed in section 5, focusing on the downscaled TCs themselves and the fields at different horizontal scales. A case study for a year with the largest variance is analyzed in section 6. The main conclusions are drawn in the last section together with a brief discussion.

2. Model description, experimental design, data, and analysis methods

a. Model description

The regional climate model iRAM developed at IPRC, University of Hawaii (Wang et al. 2003) was used in this study. It has been applied to the studies of dynamically downscaled TC activity (Stowasser et al. 2007; Zhan et al. 2011a) and other regional climate modeling efforts (Wang et al. 2007). The model uses hydrostatic, primitive equations in spherical coordinates with sigma (pressure normalized by surface pressure) as the vertical coordinate. The model equations are solved with a fourth-order conservative horizontal finite differencing scheme

on an unstaggered longitude–latitude grid system. The time integration is performed using a leapfrog scheme with intermittent application of an Euler backward scheme. The model physics include the cloud microphysics scheme of Wang (2001); a mass flux scheme for subgrid shallow convection, midlevel convection, and deep convection developed by Tiedtke (1989) with some modifications outlined in Wang et al. (2003, 2004, 2007); the radiation package developed by Edwards and Slingo (1996) and further improved by Sun and Rikus (1999); the Biosphere–Atmosphere–Transfer Scheme (BATS) developed by Dickinson et al. (1993) for land surface processes; a modified Monin–Obukhov similarity scheme for flux calculations at the ocean surface; and a nonlocal E–ε turbulence closure scheme for subgrid-scale vertical mixing (Langland and Liou 1996), which was modified to include the effect of cloud buoyancy production of turbulence kinetic energy (Wang 1999). A one-way nesting is used to update the model time integration in a buffer zone near the lateral boundaries within which the model prognostic variables are nudged to reanalysis data with an exponential nudging coefficient proposed by Giorgi et al. (1993) and later modified by Liang et al. (2001). The buffer zone is 5° in extent. More details of the model can be found in Wang et al. (2003, 2004, and 2007).

The model domain in this study covers the South China Sea (SCS) and the WNP, extending from 20°S to 59.8°N, 100°E to 160°W with a grid spacing of 0.2° in both zonal and meridional directions. The model has 28 vertical levels with relatively higher resolution in the planetary boundary layer. The lowest model level is roughly 35 m above the surface. The initial and lateral boundary conditions for iRAM were constructed using the NCEP/NCAR reanalysis (Kalnay et al. 1996), available at 2.5° × 2.5° horizontal resolution

with 17 vertical pressure levels at 6-h intervals. SSTs were obtained from the Reynolds weekly SST data at 1° × 1° horizontal resolution (Reynolds et al. 2002), interpolated onto the model grids by cubic spline interpolation in the horizontal and linear interpolation in both the vertical and time.

b. Experimental design

Four simulations were conducted with slightly different initial conditions, as shown in Table 1. They were initialized at 00 UTC on four successive days from 28 June to 1 July of each year and were run until 18UTC 31 October for 20 typhoon seasons from 1982 to 2001. The 6-hourly outputs from each experiment were analyzed for the typhoon season from 00 UTC 1 July through 18 UTC 31 October. Previous studies have shown some initial shock in the simulation and suggested a need to exclude the analysis for the spin-up time period. For example, Giorgi and Mearns (1999) presented the spin-up time of about 10 days for atmospheric fields. Note that the spin-up of the atmospheric processes is relatively much faster than that of the land surface processes. Since our model domain covers mainly the ocean areas, the spin-up could not be a serious problem as found for simulations of regional climate over land areas. We therefore ignored the effect of the spin-up time in this study.

All simulations shared exactly the same LBCs for the atmospheric fields and the same prescribed SST. The only difference is the one-day delay of the model initial time, and thus differences among these simulations would be considered as a result of small changes in the initial conditions.

Note that the control of large-scale motion on the regional simulation is purely through the lateral boundary conditions in our simulations. Although previous studies have shown the

improvements in the downscaled TC climatology and interannual variability with the use of some spectral nudging technique (e.g., Knutson et al. 2007, 2008; Bender et al. 2010), the spectral nudging would reduce the internal variability considerably (nevertheless, the simulations could be very sensitive to the nudging time scale as well, Knutson et al. 2007). Therefore, similar to Alexandru et al. (2007), the spectral nudging was not considered in our simulations in order to appreciate the internal variability in both the basic state and the synoptic scale motions.

c. Data

The best track TC data (6-hourly position and intensity) were obtained from Shanghai Typhoon Institute of China Meteorological Administration (CMA). The CMA best track data for the WNP started from 1949, but the period 1982–2001 was used in this study to verify the model simulations for the same period. In addition, we only considered TCs that reached at least the tropical storm (TS) intensity (with maximum sustained wind speed Vmax $\geq$17 m s^{-1}). The atmospheric fields from the model were compared with the NCEP/NCAR reanalysis.

d. Criteria for identifying TCs

The method for detecting and tracking the model TCs is similar to that used in earlier studies by Nguyen and Walsh (2001) and Stowasser et al. (2007) with some modifications for our model resolution. With 6-hourly model outputs, the following criteria are set for a system to be identified as a tropical storm in our simulations:

1) There must be a relative vorticity local maximum exceeding 5×10^{-5} s^{-1} at 850 hPa.
2) There must be a local minimum in sea level pressure (SLP) within a distance of 4° latitude or longitude from the vorticity maximum; this minimum pressure is defined as

the center of the model storm.

3) The azimuthal mean tangential wind speed at 850 hPa must be higher than at 300 hPa.
4) The closest local maximum in temperature averaged between 500 and 200 hPa is distinguishable and is defined as the center of the warm core. The distance between the center of the warm core and the center of the storm must not exceed 2.5° latitudes. From the center of the warm core the temperature must decrease by at least 0.5°C in all directions within a distance of 7.5°.
5) The storm must form at latitudes south of 35°N.

To be considered as a model tropical storm trajectory, a storm must last at least 2 days and have a maximum wind speed of over 17 m s^{-1} at the lowest model level during at least 2 days (not necessarily consecutive). For each storm snapshot, it is checked whether there are storms during the following 6-h period within a distance of 300 km south of 25°N or 600 km north of 25°N. If there is none, the trajectory is considered to discontinue. If any is present, the closest storm is designated to have the same trajectory as the initial storm. Cases satisfying all these criteria are referred to as TCs in this study.

e. Evaluation methods

Following Alexandru et al. (2007), the internal variability of the downscaled fields in this study is measured by the spread among the ensemble members during the simulation period, using the root-mean-square error (RMS) between the four simulations and the ensemble mean, where RMS is estimated by

$$RMS = \sqrt{\frac{1}{M}\sum_{m=1}^{M}[X_m - \langle X \rangle]^2} \qquad (1)$$

The term X_m refers to the value of a variable X for member m in the ensemble and M is the

total number of ensemble members (4 in this study). The term $\langle X \rangle$ is the ensemble mean defined as

$$\langle X \rangle = \frac{1}{M} \sum_{m=1}^{M} X_m \tag{2}$$

To separate the contributions by different horizontal scales to the error growth, the RMS^2 is divided into two components by partitioning the variable X into a large-scale variable $\overline{X}$ and a small-scale variable X' as

$$RMS^2 = \overline{RMS^2} + RMS^{2'} \tag{3}$$

where $\overline{X}$ is obtained by calculating running means over grid boxes, X' is the deviation of X from $\overline{X}$, and $\overline{RMS^2}$ and $RMS^{2'}$ are defined as the standard deviation of $\overline{X}$ and X', respectively.

These statistics are evaluated in different time intervals. When examining the relations between large-scale fields and TC frequency in terms of internal variability, we focus on SLP since a TC system can be tracked in SLP field more directly and easily than other variable in the model output.

3. Large-scale features and TC climatology

We begin with evaluation of the simulated climatological large-scale features in the 20-yr typhoon seasons to verify the performance of iRAM. Figure 1 shows the climatological mean SLP and 850 hPa relative vorticity fields from both simulations and NCEP reanalysis. The low-level vorticity field in the reanalysis shows a northwest-southeast-elongated positive belt extending from the SCS to the WNP between 5°N and 20°N with the maximum center over the SCS and negative vorticity on both sides of the positive belt. The positive vorticity belt is associated with the monsoon trough, a vital factor for TC genesis in the region (Holland

1995). The negative vorticity to the north is associated with the western North Pacific subtropical high, which plays an important role in controlling TC motion in the basin. These two main features are also shown in the long-term mean SLP field and are well captured by the model in all individual simulations and the ensemble mean, although the centers over the SCS and the western WNP are stronger in the simulations than in the reanalysis, especially for the one over the SCS.

Figure 2 shows the climatological mean vertical wind shear between 850 hPa and 200 hPa and 700 hPa specific humidity fields from the simulations and the NCEP reanalysis. The reanalysis exhibits large values of humidity and easterly vertical wind shear around the monsoon trough region. Both the pattern and magnitude of the vertical wind shear are very well reproduced in all simulations. In addition, the specific humidity pattern in the simulations is in good agreement with the reanalysis throughout most of the domain. However, the model humidity is higher than that in the reanalysis. This could be partly due to the dry bias over the warm ocean in the NCEP reanalysis (Bony et al. 1997) since the magnitude of the model specific humidity is generally comparable to the European Center for Medium Weather Forecast (ECMWF) reanalysis (ERA40, not shown), and partly due to the cumulus parameterization scheme used in the model. Nevertheless, overall, the iRAM forced by the reanalysis can capture reasonably well the large-scale features in the WNP. Note that four simulations show almost consistent distributions in the climatological mean fields, suggesting that the large-scale climatological features are not significantly affected by the internal variability in the simulations. The result is in general agreement with previous studies (e.g., Giorgi and Bi 2000).

Stowasser et al. (2007) and Zhan et al. (2011a) have demonstrated that the iRAM with a grid spacing of 0.5° in both zonal and meridional directions can reproduce reasonably well the climatology of the observed TC behavior over the WNP. Here, a higher resolution of 0.2° in both zonal and meridional directions is used. We first focus on the TC climatology from simulations with different initial conditions. As in Stowasser et al. (2007) and Zhan et al. (2011a), the frequencies of TC genesis and occurrence in the 20 typhoon seasons are calculated in each 5° longitude by 5° latitude grid box.

Figure 3 shows the spatial distributions of TC genesis frequencies for the typhoon seasons during 1982–2001 from the simulations and the CMA best track data. The TC genesis location in the simulations resembles that observed, with a maximum band of TC formation between 5°N and 25°N where the monsoon trough exists and three local maxima are located, respectively, in the SCS, around 130°E, and between 140°E and 160°E. Compared to the observation, however, the second maximum is weaker, and the third maximum is located too far to the east in the simulations.

TC occurrence is also called TC passage, which is calculated at 6-hour interval and measures how frequently TCs affect a grid box of 5° longitudes by 5° latitudes in this study. The maximum frequency of occurrence is used to infer the prevailing TC tracks. The geographical distribution of the TC occurrence frequency is also reasonably simulated (Fig. 4). The simulated TCs most frequently occur at the same latitudes from the SCS to 160°E as observed. However, there is a positive bias over the SCS in all simulations. This might be to the overly strong monsoon trough and the associated low-level cyclonic circulation simulated in that region (Fig. 1), which could lead to the excessive TC genesis and the TC track change.

A similar bias has reported in Zhan et al. (2011) with the western boundary of the model domain extended to 70^{o}E. Another bias is the underestimated frequency of occurrence north of 25°N in the simulations, notably over Korea and Japan and east of the Japan Main Island. As mentioned in Zhan et al (2011a), this discrepancy might be associated with the deficiency in the TC detection algorithm, which excludes the extratropical transitions of any tropical systems since any detected systems with a warm core more than 2.5° away from the surface center are excluded from the tropical storms in the simulations.

Note that the differences in the TC genesis frequencies near the three local maxima among the simulations are not negligible, although the general patterns are quite similar. The simulated centers in TC occurrence are not consistent with one another either. Especially, the one located to the east of the Philippines is relatively weak in the fourth simulation. In addition, the climatological mean annual TC numbers are somewhat different among the simulations, with the smallest number of TCs at 18.8 in EXP1 (375 in total) and the largest at 20.3 in EXP2 (406 in total).

Compared to the observed climatological mean of 19.5 TCs per typhoon season during 1982–2001 (390 in total), the ensemble mean from the four simulations gives the same number of TCs (19.5) per typhoon season (391 in total), which features the most realistic number of TC genesis over the WNP. We also calculate the climatological mean standard deviations between the individual simulations, the ensemble mean and the observation, and show that the deviation is the smallest between the ensemble mean and the observation. This suggests that the ensemble mean provides better downscaled information on TC genesis frequency than any individual simulation.

4. Internal variability of the downscaled WNP TC activity

In this section, we will examine the internal variability of TC activity over the WNP dynamically downscaled by the iRAM with different initial conditions. Figure 5 shows the monthly mean WNP TC numbers for the period 1982–2001 from the simulations and the observation. Although the simulated frequencies in August are uniformly higher than the observation, there is good agreement in month-to-month variation of TC genesis frequency between the simulations and the observation, with an increase from July to August, peaking in August, and a decrease from August to October. However, the model simulations show considerable internal variability even though the same lateral boundary conditions and SST are imposed as constraints of large-scale forcing. Table 2 shows climatological monthly mean RMS of the WNP TC counts in the four simulations from their ensemble mean for the typhoon season of 1982-2001. The magnitude of the internal variability in the downscaled TC genesis frequency appears to vary greatly from July to October. The largest internal variability seems to occur in October with the RMS as large as 0.57 when the difference between EXP1 and EXP2 are significant at the 95% confidence level based on *student-t* test for difference between two means from two-group samples. It should also be kept in mind that downscale experiments for individual year are independent of each other even if the starting calendar date is the same. That is, the internal variability of climatological monthly TC counts in the simulations has uncertainty. In order to assess such uncertainty, a bootstrap resampling method is further used here to obtain the probability distribution function of RMS. In our application, new sample is monthly RMS derived from four new time series of monthly TC numbers during 1982-2001, which are formed by randomly choosing one

element from four original simulations in each year as a replacement in certain time series in that year. 2000 bootstrap resamples are taken, and a statistics of interest is calculated for each group of resamples. Three useful statistics for summarizing the probability distribution are the median, lower quantile and upper quantile, shown in Table 2. The last two statistics can be regarded as a measure of the 95% confidence interval. See Efron (1979) and Ferro et al. (2005) for basic introductions to the bootstrap method and a demonstration for the benefits of using such a statistics. The greatest median monthly RMS is found in August that also exhibits wider 95% confidence interval. This suggests that the largest internal variability in the monthly downscaled TC genesis frequency occurs most likely in August not in October. However, compared to RMS probability in July and September, the internal variability in October is still large, and its median and upper quantile reach 0.30 and 0.58, respectively. This is in sharp contrast to previous findings that the signal representing internal variability induced by initial conditions weakens with the simulation length (Wu et al. 2005; Vanvyve et al. 2008). This suggests that the internal variability of the dynamically downscaled TC activity might differ significantly from other variables and thus the downscaled TC should be considered as a special case.

Figure 6 shows the interannual variability of the WNP TC numbers in each typhoon season for both the simulations and the observation from 1982 to 2001. In general, differences exist among the simulations and between the model ensemble mean and the observation. The spread of TC numbers among the ensemble members is quite large in some years. Take the year 1990 for instance. 28 TCs are produced in EXP 2, but only 14 TCs in EXP4, both of which show unrealistic numbers as compared to the observed 20 TCs. Table 3

summarizes the correlations among TC numbers in the typhoon season from the four individual simulations, the ensemble mean and the observation. The correlation coefficients among the four ensemble members vary from 0.42 to 0.77, while those between individual ensemble members and ensemble mean vary from 0.76 to 0.89. The agreement between the ensemble mean and the CMA best track data is evident with the correlation coefficient of 0.7, well above 99% confidence level, and higher than those between any individual simulation and the observation. The correlations between the simulations and the best track data of Joint Typhoon Warning Center (JTWC) are also calculated and show similar results (not shown).

A quantitative estimation of the internal variability can be obtained from the RMS for the four simulations as defined in Eq. (1). Figure 7 shows the interannual variability of the RMS for the downscaled WNP TC numbers in the typhoon season from 1982 to 2001. The RMS varies largely from 0.8 to 5.3 with a mean of 2.5 during 1982–2001. The RMS is comparable to and in some instances larger than the interannual standard deviation (4.0) of the observed TC frequency. The maximum RMS occurs in 1990, with a value of 5.3, namely 25% of the TC counts in the ensemble mean. The low correlation and high RMS among the ensemble members imply that the downscaled TC frequency exhibits strong internal variability.

A behavior similar to that of the downscaled TC frequency is also found in the downscaled TC intensity. Figure 8 shows the time series of the WNP TC power dissipation index (PDI) in the typhoon season for the simulations and the observation from 1982 to 2001. The PDI index, proposed by Emanuel (2005) to measure TC intensity, is defined as the sum of the cubic power of the maximum wind speed over the TC lifespan containing TC-force winds. The correlation coefficients between the four ensemble members and the CMA best

track data vary from 0.47 to 0.66, while the coefficient between the ensemble mean and the CMA best track data reaches 0.66. The internal variability in the downscaled TC intensity is evident, with an average RMS of 15% of the TC intensity in the ensemble mean. In particular, the maximum RMS occurs in 1982 with a value of 40% of the TC intensity in the ensemble mean.

5. Sources of uncertainties

As mentioned above, the downscaled TC genesis frequency exhibits strong internal variability, although the climatological mean large-scale environment is not very sensitive to the initial conditions. To further investigate the possible sources of uncertainties leading to the large internal variability in the downscaled TC activity, the uncertainties arising from the initial perturbations and the detection of TC-like vortices in the model are analyzed in this section. The diagnostic study of a particular case in 1990 with the largest variance is presented in the next section.

a. Uncertainties in the initial perturbations

The initial states in the four simulations contain unavoidable biases. We calculate the RMS field of SLP at 00 UTC 1 July averaged for the period 1982–2001, as shown in Fig. 9a. For a comparison of the degree of uncertainty, the RMS field of SLP averaged in the 20 typhoon seasons is shown in Fig. 9b. In general, the distribution of RMS in the initial state is similar to that averaged in the whole season, with large RMS north of 30°N and small RMS in the tropics. As expected, the RMS in the initial state is significantly smaller than that averaged in the typhoon season, although the RMS value is still comparable to each other. The former is generally less than about 40% of the latter, except in a few small regions where

the initial RMS is somewhat large. The results imply that the uncertainty in the initial state is relatively small, which will be further expatiated in the next section for a case study, and that the other uncertainties might be dominant.

b. Uncertainties in the detection of TC-like vortices

In the model, disturbances satisfying all criteria outlined in section 2d are referred to as TCs, while a system satisfying only the first five criteria is identified as an initial TC-like vortex. That is, an initial TC-like vortex is defined as a detected TC-like system without ′duration′ and ′intensity′ criteria here. Hence, a downscaled TC is mainly determined by three factors: the initial TC-like vortex, its intensity, and its duration. A question arises as to whether the large internal variability of the downscaled TC activity induced by the small initial perturbations results from the detection of the TC-like vortices. To address this question, we examine the uncertainties in the detection of TC-like vortices in all simulations.

Figure 10a shows the interannual variability of the number of the initial TC-like vortices during the typhoon season for all individual simulations and the ensemble mean from 1982 to 2001, while Fig. 10b shows the interannual variability of the numbers of the detected TC-like vortices lasting not less than 2 days but without the ′intensity′ criterion. It is clear that both of the vortex numbers are very sensitive to the initial perturbations and show pronounced differences among the ensemble members. Especially, the effect of the perturbations on the number of the detected TC-like vortices not less than 2 days but without the ′intensity′ criterion is more significant. In terms of the effects of the initial perturbations on the duration (Fig. 10b) and intensity (Fig. 6) of the TC-like vortices, the number of vortices lasting not less than 2 days varies by about 5%~30% of the ensemble mean, which is at about the same

level as the detected TC numbers. This finding indicates that the development of a TC-like vortex including its formation and intensification is more vulnerable to the variations in the initial conditions than its initial genesis stage. Moreover, about three quarters of TC-like vortices lasting longer than 2 days but without satisfying the 'intensity' criterion to be identified as TCs developed eventually. In this sense, the large internal variability of the downscaled TC genesis frequency among the simulations may result from the difference in the transition from less organized disturbances to the well-organized coherent TC structure. This transition is likely to be a highly nonlinear process and is sensitive to small differences in the initial conditions.

6. A case study for 1990 with the largest variance

As shown in Fig. 7, the internal variability in 1990 is the largest with an RMS reaching 25% of the ensemble mean. In this section, the internal variability of the downscaled TC activity in year 1990 is further examined to help understand the uncertainties in the model simulations.

Figure 11 shows the SLP fields at 12 UTC 26 July 1990 for the simulations and the NCEP reanalysis. Good agreement in the large-scale features is noted for the simulations and the reanalysis, with the western North Pacific subtropical high in the northeast of the model domain and the TC activity in the WNP. This agreement among the simulations might be made possible by the design that the model is forced by the same LBC. However, different patterns in the TC activity are evident. Two TCs occurred in EXP 2 and EXP 4, similar to those in the reanalysis with one at 144.3°E, 19.5°N and the other at 156.0°E, 31.0°N, while only one TC formed in EXP1 and EXP3. Besides the TC numbers, the four simulations also

show large differences in the location and intensity of the downscaled TCs on this particular day. This suggests that due to their highly nonlinear nature, the dynamically downscaled individual TC events may have quite different responses to slightly different initial conditions at any given time during the time integration of the model.

Differences in the downscaled TC activity in the simulations can be further demonstrated in the eddy kinetic energy (EKE) fields, calculated based on the difference between the original state and its basic state defined as an 11-day running mean of the original state. Figure 12 shows the EKE at 850 hPa averaged in the typhoon season of 1990. In all simulations, there appears a northwest-southeast-oriented large EKE band, similar to the one in the reanalysis (Fig. 12f). However, both EXP3 and EXP4 show relatively greater EKE than the other two simulations. Moreover, the maximum EKE center in EXP4 is located to the northwest of those in other three simulations. These differences suggest that small perturbations in the initial conditions significantly change the model statistics at relatively small-scale motions.

To further understand the model internal variability, we decomposed the horizontal SLP field into the large-scale component and the small-scale component by calculating running means over grid boxes. We used grid boxes of a mere 50×50 to represent waves longer than 1000 km. When calculating the differences between the unfiltered and filtered fields, we can obtain components containing only scales with shorter wavelengths. Figures 13 and 14 show the filtered SLP anomalies from the ensemble mean in the four simulations and the filtered SLP in the ensemble mean and the NCEP reanalysis averaged in the typhoon season of 1990 with wavelength longer than 1000 km and shorter than 1000 km, respectively. The

large-scale fields in Fig. 13 show small differences between the ensemble mean and the reanalysis, similar to the climatological mean SLP fields shown in Fig. 1. The anomalies among the individual simulations are large over the monsoon trough region and the western North Pacific subtropical high region. For the small-scale fields (Fig. 14), the remarkable differences in the simulations mainly appear the TC active region as shown in Fig. 4. Compared the anomaly values with the original values of SLP in Figs 13 and 14, the large-scale anomalies are quite small while the small-scale anomalies are comparable to the filtered SLP with wavelength shorter than 1000 km, indicating that the effect of the initial conditions on the downscaled small-scale statistics is indeed significant.

To examine the sources of the internal variability, the differences of SLP between EXP1 and other simulations valid at 00 UTC 1 July 1990 are shown in Fig. 15. Since EXP1 was initiated at 00 UTC 1 July of each year, the differences in Fig. 15 are equivalent to those between the reanalysis and the simulations if the additional biases induced by the interpolation procedure are neglected. Generally, SLP in the simulations is uniformly 1~3 hPa higher than that in the reanalysis except for in the area west of 110°E after some short time integrations. The differences of SLP in the ensemble mean are the smallest among all individual simulations. Further examination for other years (not shown) demonstrates that the magnitude of the initial differences is similar to one another. This implies that the internal variability of the downscaled TC activity exists independently of the amplitude of the initial perturbations, consistent with the results of Giorgi and Bi (2000).

The temporal evolution of domain-averaged variance for SLP between individual simulations and the ensemble mean in 1990 is shown in Figs. 16a~c. The variance is

averaged in the region 0°–40°N and 105°E–180°. In order to compare the internal variability in different years, the temporal evolution of domain-averaged variance in 1985, with the minimum internal variability (Fig. 7), is presented in Figs. 16d~f. For the year 1990, the variance in individual simulations essentially oscillates around 0~36 hPa, and does not significantly reduce with time (Fig. 16a). The oscillation also shows a similar behavior in all simulations, which is tied to the synoptic scale variability, with time scales from several to tens of days. This is essentially due to the same level of forcing from synoptic scale perturbations through the lateral boundaries in all simulations. However, the magnitude of variance in the individual simulation differs significantly from one another at any given time. The inconsistency in magnitude among the simulations implies the differences in the day-to-day model solutions induced by the initial conditions as a result of the development of nonlinear atmospheric instabilities. When we compare Fig. 16a with Figs. 16b and 16c, we can see that horizontal scales with wavelengths longer than 1000 km contribute largely to the magnitude and variability of variance in the unfiled field.

Further examinations of daily SLP field show that the internal variability on large scales is contributed by changes in the western North Pacific subtropical high (not shown), while that on small scales is greatly associated with the TC activity (e.g., location, intensity, and frequency). The latter can also be seen in Fig. 11, which shows a large variability of the downscaled TC activity in the simulations. Similar to the results in 1990, the total variability in 1985 is also originated from that on large scales, but it generally exhibits smaller values on both large scales and small scales than those in 1990. This is consistent with the smallest variability of the downscaled TC activity in 1985. These results suggest that the slight

difference in the initial conditions can change the day-to-day model solutions. The internal variability of the downscaled TC activity on interannual time scales is associated with the internal variability on both large scales and small scales in the simulations. They both significantly modulate the transition from less organized disturbances to the well-organized coherent TC structure. In this sense, the large internal variability of the downscaled TC activity results from the development of nonlinear atmospheric instabilities, which is controlled by the large scale settings of the seasons, and the random nature of TC genesis under favorable environmental conditions.

7. Conclusion and discussion

In this study, efforts have been made to demonstrate the internal variability of dynamically downscaled TCs over the WNP in a regional climate model. Four simulations have been conducted for 20 typhoon seasons from 1982 to 2001 using the IPRC regional atmospheric model (iRAM), which is driven by the same LBCs for the atmospheric fields and prescribed weekly SST. The only difference in these simulations is in the initial time delayed by 1 day.

The results show that all simulations can capture the large-scale features in the WNP reasonably well, and can realistically reproduce the observed geographical distributions of TC genesis and the frequency of occurrence. However, the difference in the TC climatology is not negligible among the simulations, although the climatological mean large-scale features are quite similar. Both the local maxima in the frequencies of TC genesis and occurrence and the climatological mean TC numbers show differences among the simulations. Such differences stem mainly from the internal variability of the model atmosphere associated with

the slightly different initial conditions.

As synoptic-scale storms, the formation/genesis of TCs involves complex nonlinear and multiscale interactions. On the seasonal timescale, the internal variability of the downscaled TC genesis frequency varies considerably from July to October, peaking in August and the second in October. This is inconsistent with previous findings that the signal representing internal variability induced by initial conditions weakens with time so that confidence in the simulations increases with the simulation length (Wu et al. 2005; Vanvyve et al. 2008). On the interannual timescale, the correlation coefficient between the downscaled TC genesis frequencies from any two of the simulations varies from 0.42 to 0.77. The RMS is comparable to and in some instances even larger than the interannual variability of the observed TC frequency, with the maximum value in 1990, amounting to 25% of the TC number in the ensemble mean.

Because of the same level of synoptic variability through the lateral boundaries, all simulations share similar organized structures in model internal variability. The large-scale features display relatively small differences among the simulations, while the small-scale features are significantly affected by the initial conditions. The internal variability of the downscaled TC activity is found to be insensitive to the amplitude and the pattern of the initial perturbations. Our results show that the development of a TC-like vortex is more vulnerable to the variations in the initial conditions than its initial genesis stage. The large internal variability of the downscaled TC genesis frequency among the simulations may result mainly from the difference in the transition from less organized disturbances to the well-organized coherent structure. This transition is likely to be a highly nonlinear process

and is sensitive to the small differences in the initial conditions, as demonstrated to the sensitivity in the detection algorithm of TC-like vortices in the model simulations. This is in sharp contrast to previous studies (Giorgi and Bi 2000; Vannitsem and Chome 2005; Wu et al. 2005; Vanvyve et al. 2008), which indicated that small perturbations in the initial conditions do not appear to significantly change the RCM solution.

The large-scale environmental conditions, such as low-level vorticity, vertical wind shear, mid-level humidity, and thermodynamic stability, play important roles in the interannual variability in TC genesis frequency. A natural question arises as to whether the internal variability of the environmental conditions contributes to the difference in TC counts among the ensemble members. This is discussed by examining the differences in RMS fields in vertical wind shear and mid-level specific humidity. The differences in RMS fields of daily vertical wind shear and mid-level relative humidity between year 1990 with the largest TC variability and year 1985 with the smallest one are shown in Figs.17a, b. As expected, the RMS fields of the two environmental conditions in 1990 are larger than those in 1985 in most of the model domain, suggesting that the large internal variability in dynamically downscaled TC counts might be partially associated with the differences in large-scale environmental conditions. Further, we defined four large-variability years (1989, 1990, 1995 and 1997, with RMS $\geq$ 1 standard deviation) and four small-variability years (1985, 1988, 1996 and 1999, with RMS $\leq$ -1 standard deviation) according to the normalized time series of Fig. 7. The composite differences between large-variability and small-variability years are shown in Figs. 17c, d. The results are similar to those from two extreme years as shown in Figs.17a, b. However, the differences are not statistically significant even at 90% confidence level based

on the Student's t test. Since the large-scale conditions are only necessary but not sufficient conditions for TC genesis, the internal variability of the environmental conditions might have contributed to the difference in TC counts among the ensemble members. Such an effect could not be sufficient to explain the difference in TC genesis among the ensemble simulations. In this sense, the large internal variability of the downscaled TC genesis frequency among the ensemble simulations may result predominantly from the difference in the transition from less organized disturbances to the well-organized coherent TC structure.

Our results also show that in contrast to individual simulations, the ensemble mean provides the better downscaled information on seasonal and interannual frequencies of TC genesis and occurrence. The correlation coefficient and the standard deviation between the ensemble mean and the observation show robust improvement although only a minimum of four ensemble members are considered in this study. The conclusion is consistent with the previous study by Chen and Lin (2011) who predicted the TC counts using a global model with four ensemble members. A future study is needed to address the question as to whether the main conclusions here would remain unchanged when more ensemble members are considered. Nevertheless, the single realization from a regional model in some earlier climate change assessment studies (Stowasser et al. 2007; Knutson et al. 2007, 2008; Bender et al. 2010; and among others) might impose limitations since they do not take into account the internal variability.

Acknowledgments: This work is supported by the National Science Council of Taiwan Grants NSC 98-2111–M-002-008–MY3. Ruifen Zhan acknowledges the support from the NSFC grants 40805040 and 41075071. Yuqing Wang is partly supported by the NSF grant

ATM-0754029 awarded to the University of Hawaii. Additional support has been provided by the Japan Agency for Marine-Earth Science and Technology (JAMSTEC), NASA, and NOAA through their sponsorship of the International Pacific Research Center at the University of Hawaii, which hosted short visits by Li Yu and Ruifen Zhan.

References

Alexandru, A., R. de Elia, and R. Laprise, 2007: Internal variability in regional climate downscaling at the seasonal scale. *Mon. Wea. Rev*., **135**, 3221–3238.

Bender, M. A., T. R. Knutson, R. E. Tuleya, J. J. Sirutis, G. A. Vecchi, S. T. Garner, and I. Held, 2010: Modeled impact of anthropogenic warming on the frequency of intense Atlantic hurricanes**.** *Science*, **327**, 454–458, doi:10.1126/science.1180568.

Bony, S., Y. Sud, K. M. Lau, J. Susskind, and S. Saha, 1997: Comparison and satellite assessment of NASA/DAO and NCEP–NCAR reanalyses over tropical ocean: Atmospheric hydrology and radiation. *J. Climate*, **10**, 1441–1462.

Camargo, S. J., H. L. Li, and L. Q. Sun, 2007: Feasibility study for downscaling seasonal tropical cyclone activity using the NCEP regional spectral model. *Int. J. Climatol.*, **27**, 311–325.

Caya, D., and S. Biner, 2004: Internal variability of RCM simulations over an annual cycle. *Climate Dyn*., **22**, 33–46.

Chen, J. H., and S. J. Lin, 2011: The remarkable predictability of inter-annual variability of Atlantic hurricanes during the past decade. *Geophys. Res. Lett.*, **38**, L11804, doi:10.1029/2011GL047629.

Christensen, O. B., M. A. Gaertner, J. A. Prego, and J. Polcher, 2001: Internal variability of regional climate models. *Climate Dyn.*, **17,** 875–887.

Dickenson, R. E., R. M. Errico, F. Giorgi, and G. T. Bates, 1989: A regional climate model for western United States. *Clim. Change*, **15**, 383–422.

Dickinson, R. E., A. Henderson-Sellers, and P. J. Kennedy, 1993: Biosphere–atmosphere transfer scheme (BATS) version 1e as coupled to the NCAR Community Climate Model.

NCAR Tech. Note NCAR/TN-387STR, National Center for Atmospheric Research, Boulder, CO, 72 pp.

Edwards, J. M., and A. Slingo, 1996: Studies with a flexible new radiation code. I: Choosing a configuration for a large-scale model. *Quart. J. Roy. Meteor. Soc.*, **122**, 689–719.

Efron, B., 1979: Bootstrap methods: another look at the jackknife. The annals of Statistics, 7(1): 1-26.

Emanuel, K., 2005: Increasing destructiveness of tropical cyclones over the past 30 years. *Nature*, **436**, 686–688.

Ferro, C. A. T., A. Hannachi, D. B. Stephenson, 2005: Simple Nonparametric Techniques for Exploring Changing Probability Distributions of Weather. *J. Climate*, **18,** 4344–4354.

Feser, F., and H. von Storch, 2008: A dynamical downscaling case study for typhoons in Southeast Asia using a regional climate model. *Mon. Wea. Rev.*, **136**, 1806–1815.

Giorgi, F., and G. T. Bates, 1989: The climatological skill of a regional model over complex terrain. *Mon. Wea. Rev.*, **117**, 2325–2347.

——, and L. O. Mearns, 1999: Introduction to special section: Regional climate modeling revisited, *J. Geophys. Res.*, **104**(D6), 6335–6352, doi:10.1029/98JD02072.

——, and X. Bi, 2000: A study of internal variability of a regional climate model. *J. Geophys. Res.*, **105**, 29503–29521.

——, M. R. Marinucci, G. T. Gates, and G. De Canio, 1993: Development of a second-generation regional climate model (RegCM2). Part II: Convective processes and assimilation of lateral boundary conditions. *Mon. Wea. Rev.*, **121**, 2814–2832.

Holland, G. J., 1995: Scale interactions in the western Pacific monsoon. *Meteor. Atmos. Phys.*,

56, 57–79.

Knutson, T. R., J. J. Sirutis, S. T. Garner, I. M. Held, and R. E. Tuleya, 2007: Simulation of the recent multidecadal increase of Atlantic hurricane activity using an 18-km-grid regional model. *Bull. Am. Meteorol. Soc.,* **88**, 1549–1565.

——, ——, ——, G. A. Vecchi, and I. Held, 2008: Simulated reduction in Atlantic hurricane frequency under twenty-first-century warming conditions. *Nature Geosci.,* **1,** 359–364.

Landman, W. A., A. Seth and S. J. Camargo, 2005: The effect of regional climate model domain choice on the simulation of tropical cyclone-like vortices in the southwestern Indian Ocean. *J. Climate*, **18**, 1263–1274.

Langland, R. H., and C. S. Liou, 1996: Implementation of an E–ε, parameterization of vertical subgrid-scale mixing in a regional model. *Mon. Wea. Rev*., **124**, 905–918.

Liang, X., K. E. Kunkel, and A. N. Samel, 2001: Development of a regional climate model for U.S. Midwest applications. Part I: Sensitivity to buffer zone treatment. *J. Climate,* **14**, 4363–4378.

Nguyen, K. C., and K. J. E. Walsh, 2001: Interannual, decadal, and transient greenhouse simulation of tropical cyclone–like vortices in a regional climate model of the South Pacific. *J. Climate*, **14**, 3043–3054.

Nicolis, C., 2007: Dynamics of model error: The role of the boundary conditions. *J. Atmos. Sci*., **64**, 204–215.

Nutter, P., D. Stensrud, and M. Xue, 2004: Effects of coarsely resolved and temporally interpolated lateral boundary conditions on the dispersion of limited-area ensemble forecasts. *Mon. Wea. Rev.*, **132**, 2358–2377.

Seth, A., and F. Giorgi, 1998: The effects of domain choice on summer precipitation simulation and sensitivity in a regional climate model. *J. Climate*, **11**, 2698–2712.

Stowasser, M., Y. Wang, and K. P. Hamilton, 2007: Tropical cyclone changes in the western North Pacific in a global warming scenario. *J. Climate*, **20**, 2378–2396.

Sun, Z., and L. Rikus, 1999: Improved application of exponential sum fitting transmissions to inhomogeneous atmosphere. *J. Geophys. Res.*, **104**, 6291–6303.

Tiedtke, M., 1989: A comprehensive mass flux scheme for cumulus parameterization in large-scale models. *Mon. Wea. Rev.*, **117**, 1779–1800.

Vannitsem, S. and F. Chome, 2005: One-way nested regional climate simulations and domain size, *J. Climate*, **18**, 229–233.

Vanvyve, E., N. Hall, C. Messager, S. Leroux, and J.P. Ypersele, 2008: Internal variability in a regional climate model over West Africa. *Clim. Dyn.*, **30**, 191–202.

Walsh, K. J. E. and J. Syktus, 2003: Simulations of observed interannual variability of tropical cyclone formation east of Australia. *Atmos. Sci. Lett.*, **4**, 28–40.

——, K. C. Nguyen, and J. L. McGregor, 2004: Fine-resolution regional climate model simulations of the impact of climate change on tropical cyclones near Australia. *Clim. Dyn.*, **22**, 47–56.

Wang, Y., 1999: A triply nested movable mesh tropical cyclone model with explicit cloud microphysics—TCM3. BMRC Res. Rep. 74, Bureau of Meteorology Research Centre, Melbourne, Australia, 81 pp.

——, 2001: An explicit simulation of tropical cyclones with a triply nested movable mesh primitive equation model: TCM3. Part I: Model description and control experiment. *Mon.*

Wea. Rev., **129,** 1370–1394.

——, O. L. Sen, and B. Wang, 2003: A highly resolved regional climate model (IPRC_RegCM) and its simulation of the 1998 severe precipitation events over China. Part I: Model description and verification of simulation. *J. Climate*, **16**, 1721–1738.

——, L. R. Leung, J. L. McGregor, D. K. Lee, W. C. Wang, Y. H. Ding, and F. Kimura, 2004: Regional climate modeling: Progress, challenges and prospects. *J. Meteor. Soc. Japan*, **82**, 1599–1628.

——, S.-P. Xie, H.-M. Xu, and B. Wang, 2004: Regional model simulations of marine boundary layer clouds over the Southeast Pacific off South America. Part I: Control experiment. *Mon. Wea. Rev.*, **132**, 274–296.

——, L. Zhou, and K. Hamilton, 2007: Effect of convective entrainment/detrainment on simulation of tropical precipitation diurnal cycle. *Mon. Wea. Rev.*, **135**, 567–585.

Warner, T. T., R. A. Peterson, and R. E. Treadon, 1997: A tutorial on lateral boundary conditions as a basic and potentially serious limitation to regional numerical weather prediction. *Bull. Amer. Meteor. Soc.*, **78,** 2599–2617.

Weisse, R., H. Heyen, and H. von Storch, 2000: Sensitivity of a regional atmospheric model to a sea state–dependent roughness and the need of ensemble calculations. *Mon. Wea. Rev.*, **128**, 3631–3642.

Wu, W., A. H. Lynch, and A. Rivers, 2005: Estimating the uncertainty in a regional climate model related to initial and lateral boundary conditions. *J. Climate*, **18**, 917–933.

Zhan, R. F., Y. Wang, and C. C. Wu, 2011a: Impact of SSTA in East Indian Ocean on the frequency of Northwest Pacific tropical cyclones: A regional atmospheric model study, *J.*

Climate, (submitted).

——, ——, and X. Lei, 2011b: Contributions of ENSO and East Indian Ocean SSTA to the interannual variability of Northwest Pacific tropical cyclone frequency. *J. Climate*, **24**, 509–521.

List of Tables

Figure Captions

Figure 1. Climatological mean 850 hPa relative vorticity (10^{-5} s^{-1}, shaded) and sea level pressure (SLP, hPa, contour) fields averaged in the typhoon season of 1982–2001 from the simulations and the NCEP reanalysis.

Figure 2. The same as in Figure 1, but for zonal wind vertical shear between 200 hPa and 850 hPa (m s^{-1}, shaded) and 700 hPa specific humidity (10^{-3} kg kg^{-1}, contour).

Figure 3. Simulated and observed frequencies of TC genesis (number per year) in each 5° lon. × 5° lat. grid box for a typhoon season averaged in 1982-2001.

Figure 4. The same as in Figure 3, but for the frequency of TC occurrence (number per year).

Figure 5. Climatological mean seasonal variability of monthly TC numbers in typhoon season from four simulations, ensemble mean, and CMA best track data averaged in the period 1982-2001.

Figure 6. Interannual variability of the downscaled TC numbers in the typhoon season from four simulations, ensemble mean, and CMA best track data for the period 1982–2001.

Figure 7. Interannual variability of RMS of the WNP TC numbers in the simulations from their ensemble mean for the typhoon season of 1982–2001.

Figure 8. The same as in Figure 6, but for the power dissipation index (PDI, 10^{12} m^3 s^{-3}) of simulated and observed WNP TCs.

Figure 9. RMS fields of SLP from the ensemble mean (a) at 00 UTC 1 July and (b) in the typhoon season averaged in the period 1982–2001.

Figure 10. Numbers of TC-like vortices during the typhoon season in the four simulations and the ensemble mean: (a) Initial TC-like vortices without duration and intensity

constraints; (b) TC-like vortices lasting not less than 2 days but without intensity constraint.

Figure 11. SLP fields at 12 UTC 26 July 1990 in the simulations and the NCEP reanalysis.

Figure 12. EKE at 850 hPa (m^2 s^{-2}) averaged in the typhoon season of 1990.

Figure 13. Filtered SLP anomalies from the ensemble mean in the four simulations, and filtered SLP in the ensemble mean and the NCEP reanalysis with wavelength longer than 1000 km averaged in the typhoon season of 1990.

Figure 14. The same as in Figure 13, but for filtered SLP anomalies in all simulations and filtered SLP in the ensemble mean with wavelength shorter than 1000 km.

Figure 15. Differences in SLP fields between EXP1 and other simulations at 00 UTC 1 July 1990.

Figure 16. Domain-averaged variance in SLP (hPa) between the individual simulations and their ensemble mean for the largest variance year 1990 (left) and the smallest variance year 1985(right): unfiltered (top), large-scale with wavelength longer than 1000 km (middle), and small-scale with wavelength shorter than 1000 km (bottom).

Figure 17. Differences in the RMS fields of daily zonal wind vertical shear between 200 hPa and 850 hPa and 700 hPa specific humidity between year 1990 and year 1985 (a, b), and between the large variance and small variance years (c, d), see text for detals.

Table 1. Summary of the numerical simulations with different initial conditions

Name	Simulated period
EXP1	00UTC01Jul-18UTC31Oct
EXP2	00UTC30Jun-18UTC31Oct
EXP3	00UTC29Jun-18UTC31Oct
EXP4	00UTC28Jun-18UTC31Oct
EnsM	Ensemble mean: 01Jul-31Oct

Table 2. Climatological monthly mean RMS of the WNP TC counts in the simulations from their ensemble mean for the typhoon season of 1982-2001. Three statistics, median (0.5), lower quantile (0.05), and upper quantile (0.95), are used for summarizing the probability distribution of uncertainty in RMS based on bootstrap resampling method.

	Original	**Median**	**Lower quantile**	**Upper quantile**
Jul	0.31	0.25	0.07	0.48
Aug	0.18	0.36	0.11	0.70
Sep	0.22	0.28	0.09	0.54
Oct	0.57	0.30	0.09	0.58

Table 3. Correlation coefficients between the downscaled TC numbers in the typhoon season among the four simulations, the ensemble mean, and the CMA best track data for the period 1982–2001. The significant coefficients at 99% confidence level (±0.56) are in bold.

	EXP1	**EXP2**	**EXP3**	**EXP4**	**EnsM**	**CMA**
EXP1	**1**					
EXP2	**0.59**	**1**				
EXP3	**0.62**	**0.77**	**1**			
EXP4	0.42	**0.56**	0.52	**1**		
EnsM	**0.77**	**0.89**	**0.89**	**0.76**	**1**	
CMA	0.52	**0.66**	**0.58**	**0.56**	**0.70**	**1**

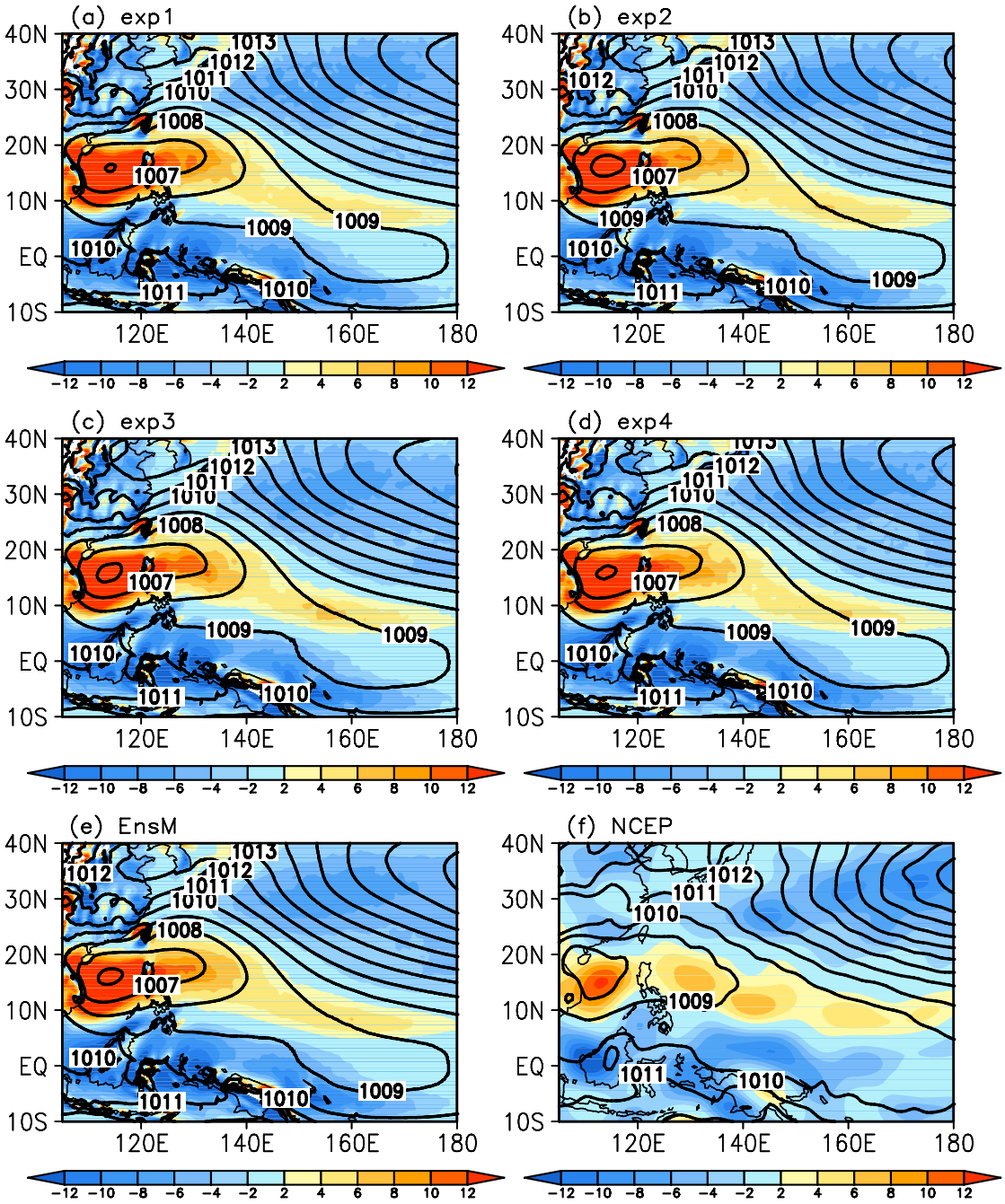

Figure 1. Climatological mean 850 hPa relative vorticity (10^{-5} s^{-1}, shaded) and sea level pressure (SLP, hPa, contour) fields averaged in the typhoon season of 1982–2001 from the simulations and the NCEP reanalysis.

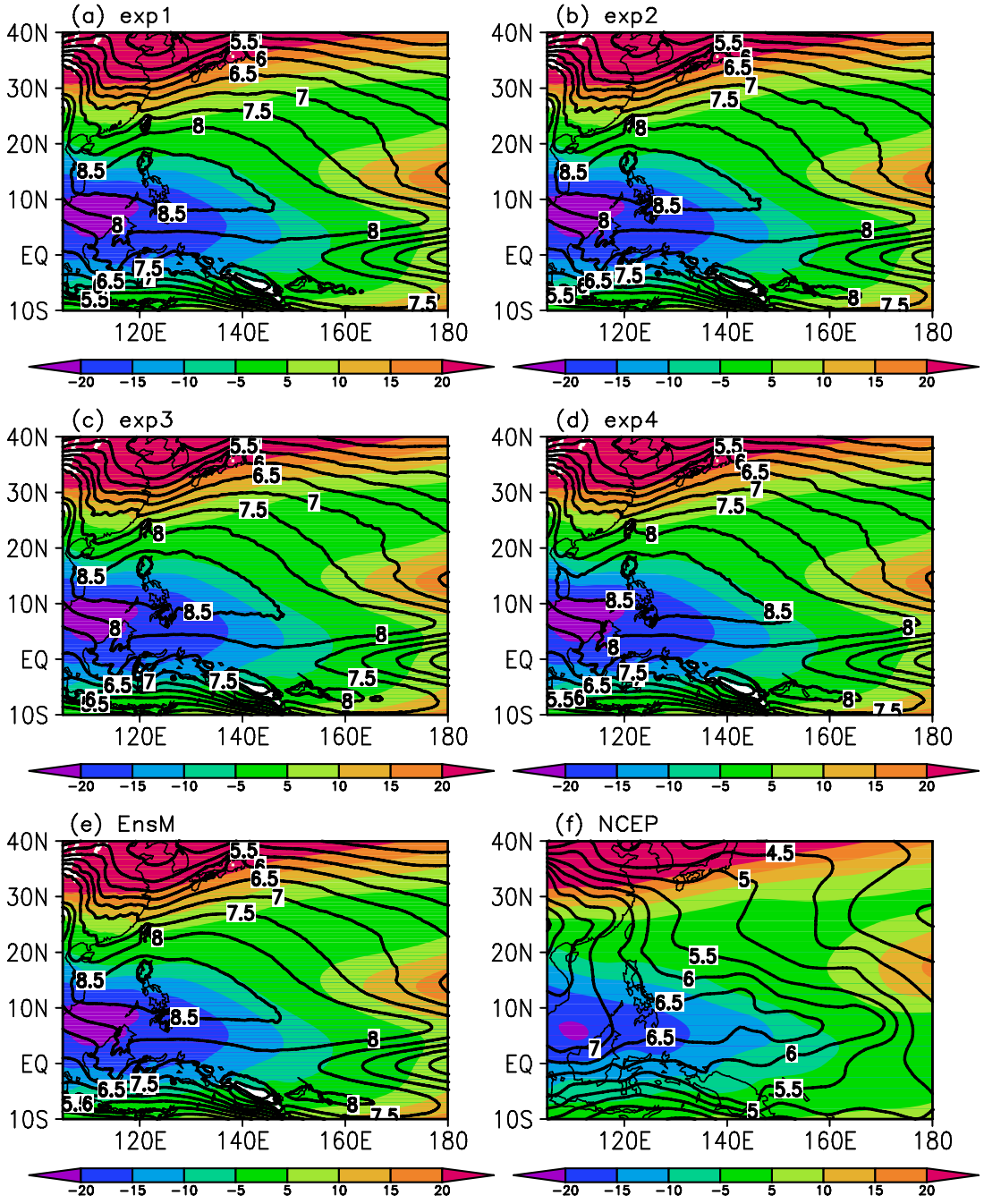

Figure 2. The same as in Figure 1, but for zonal wind vertical shear between 200 hPa and 850 hPa (m s^{-1}, shaded) and 700 hPa specific humidity (10^{-3} kg kg^{-1}, contour).

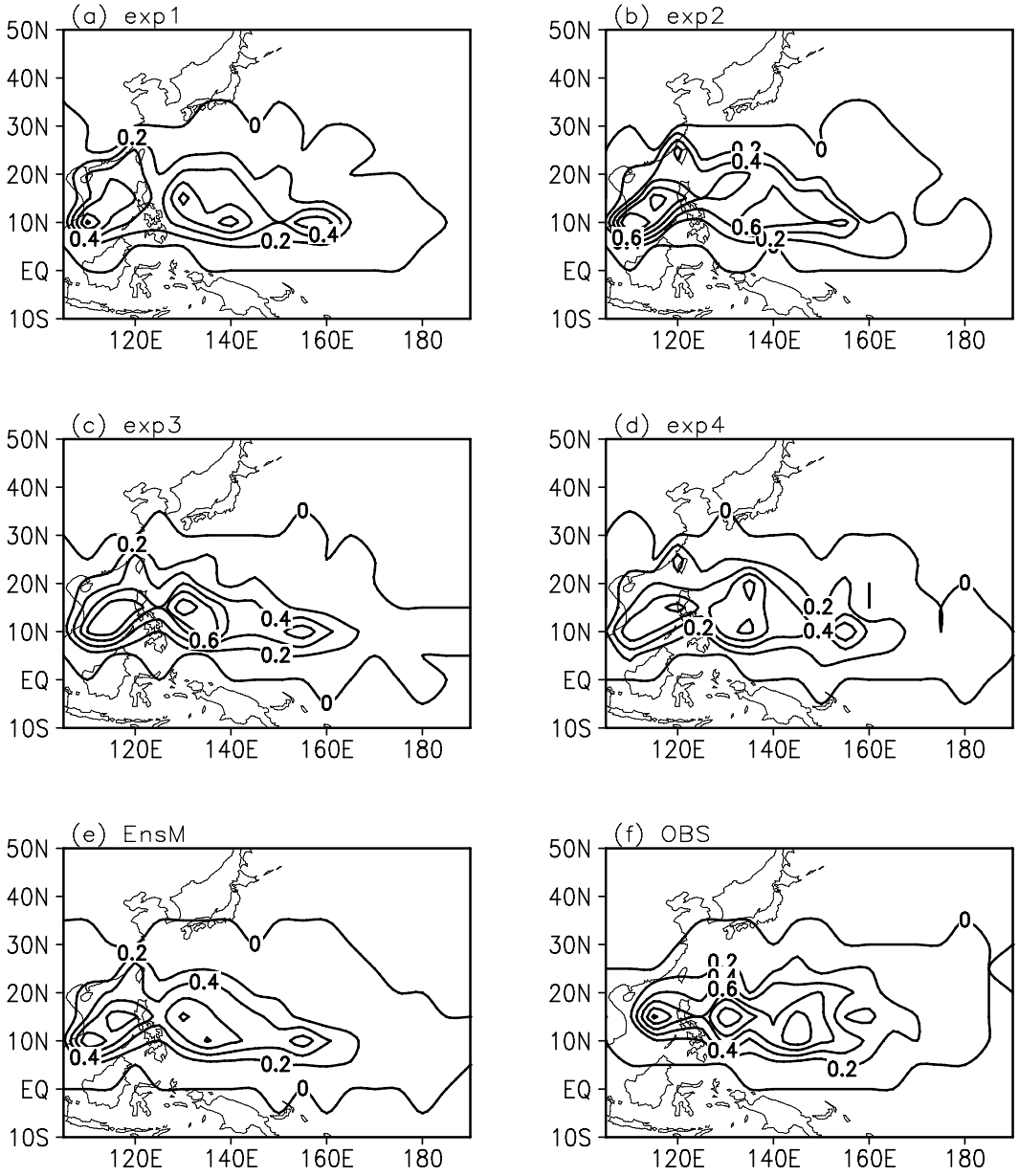

Figure 3. Simulated and observed frequencies of TC genesis (number per year) in each 5° lon. × 5° lat. grid box for a typhoon season averaged in 1982-2001.

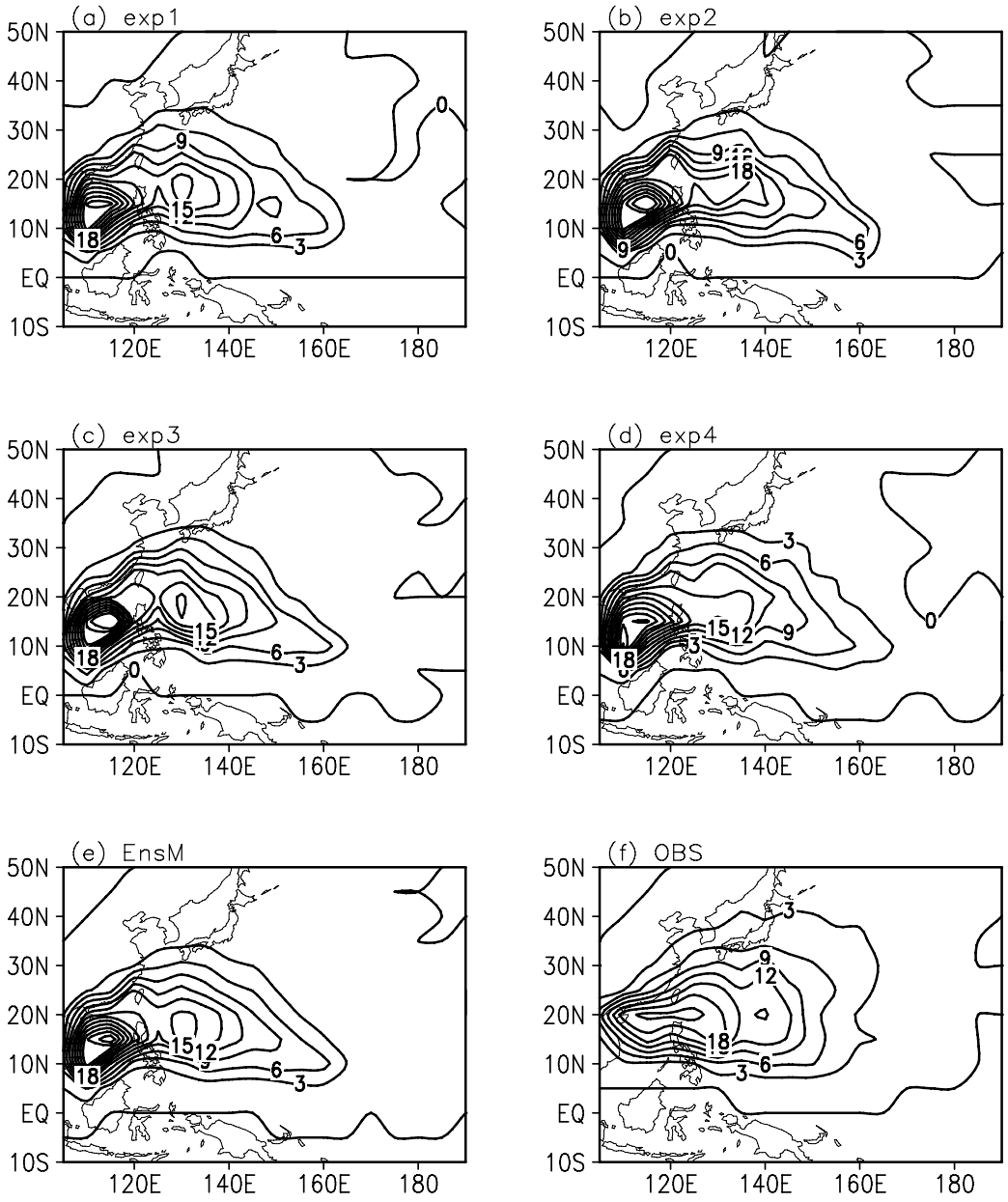

Figure 4. The same as in Figure 3, but for the frequency of TC occurrence (number per year).

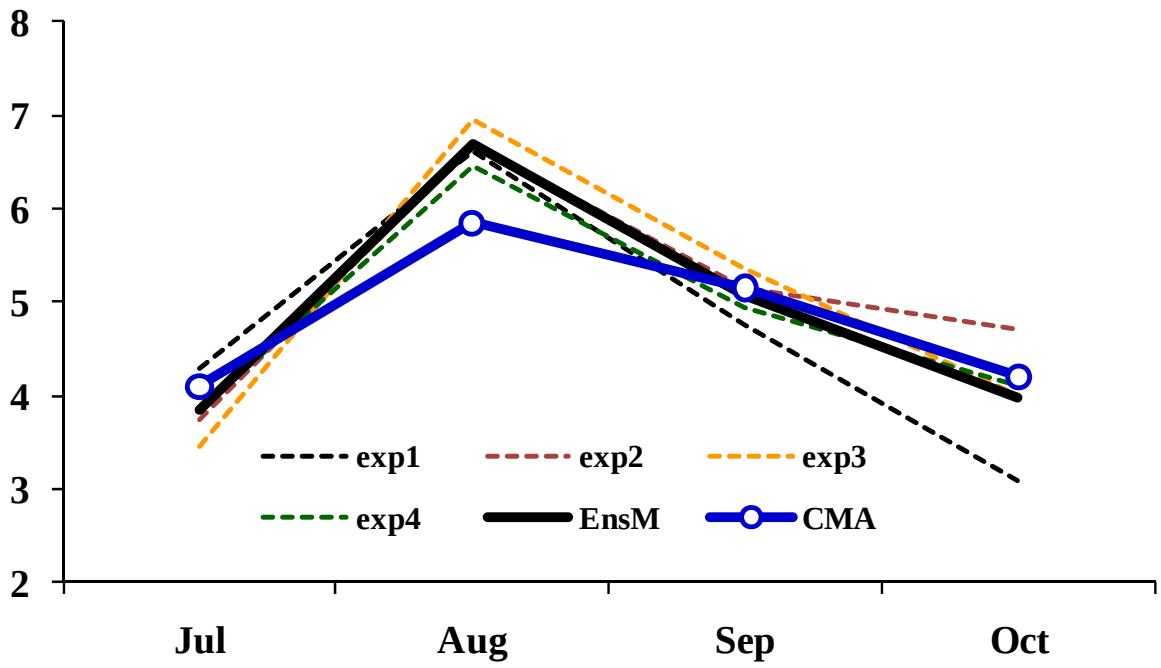

Figure 5. Climatological mean seasonal variability of monthly TC numbers in typhoon season from four simulations, ensemble mean, and CMA best track data averaged in the period 1982–2001.

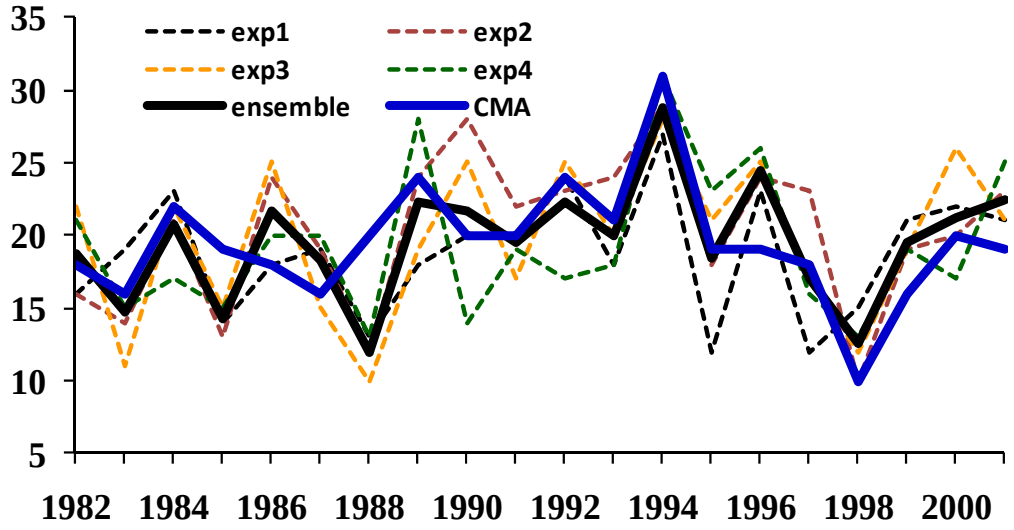

Figure 6. Interannual variability of the downscaled TC numbers in the typhoon season from four simulations, ensemble mean, and CMA best track data for the period 1982–2001.

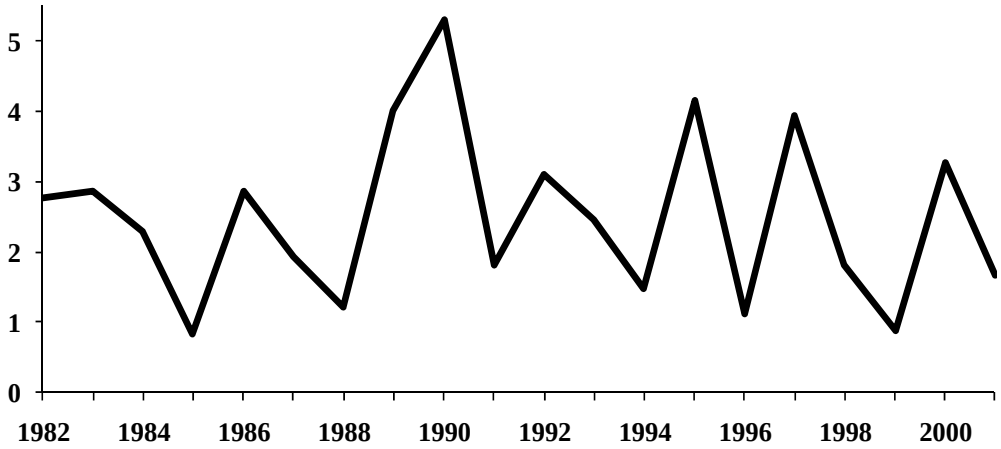

Figure 7. Interannual variability of RMS of the WNP TC numbers in the simulations from their ensemble mean for the typhoon season of 1982-2001.

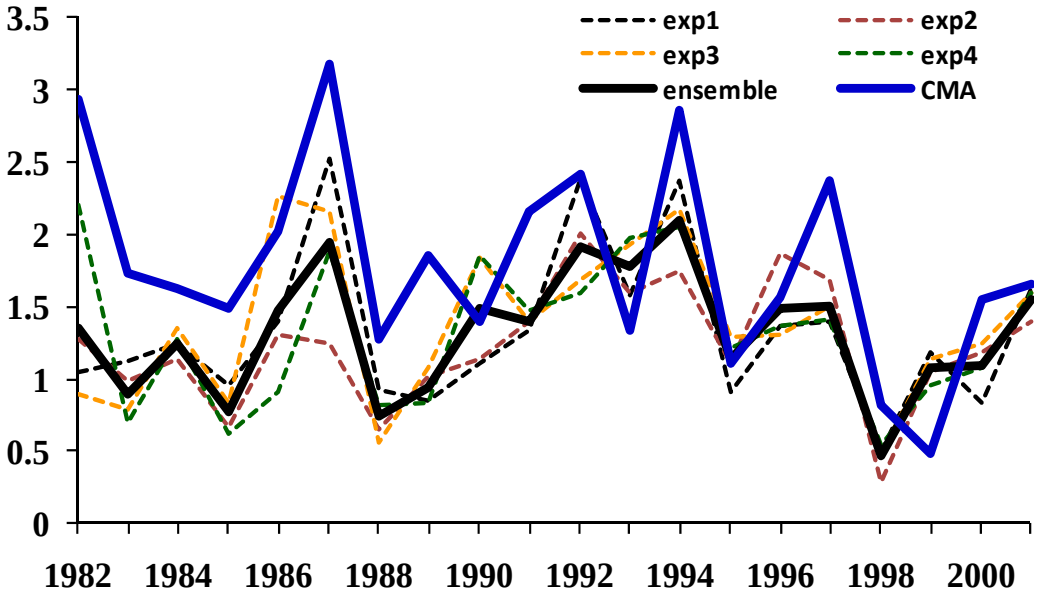

Figure 8. The same as in Figure 6, but for the power dissipation index (PDI, 10^{12} m^3 s^{-3}) of simulated and observed WNP TCs.

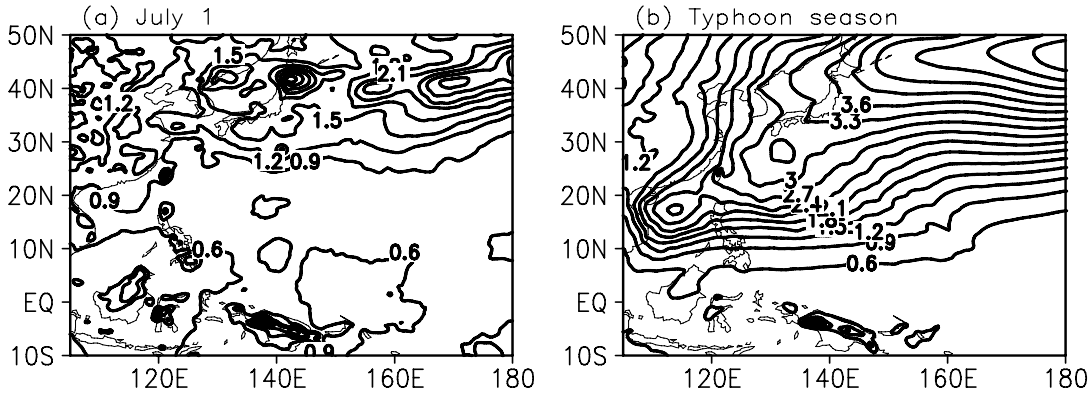

Figure 9. RMS fields of SLP from the ensemble mean (a) at 00 UTC 1 July and (b) in the typhoon season averaged in the period 1982–2001.

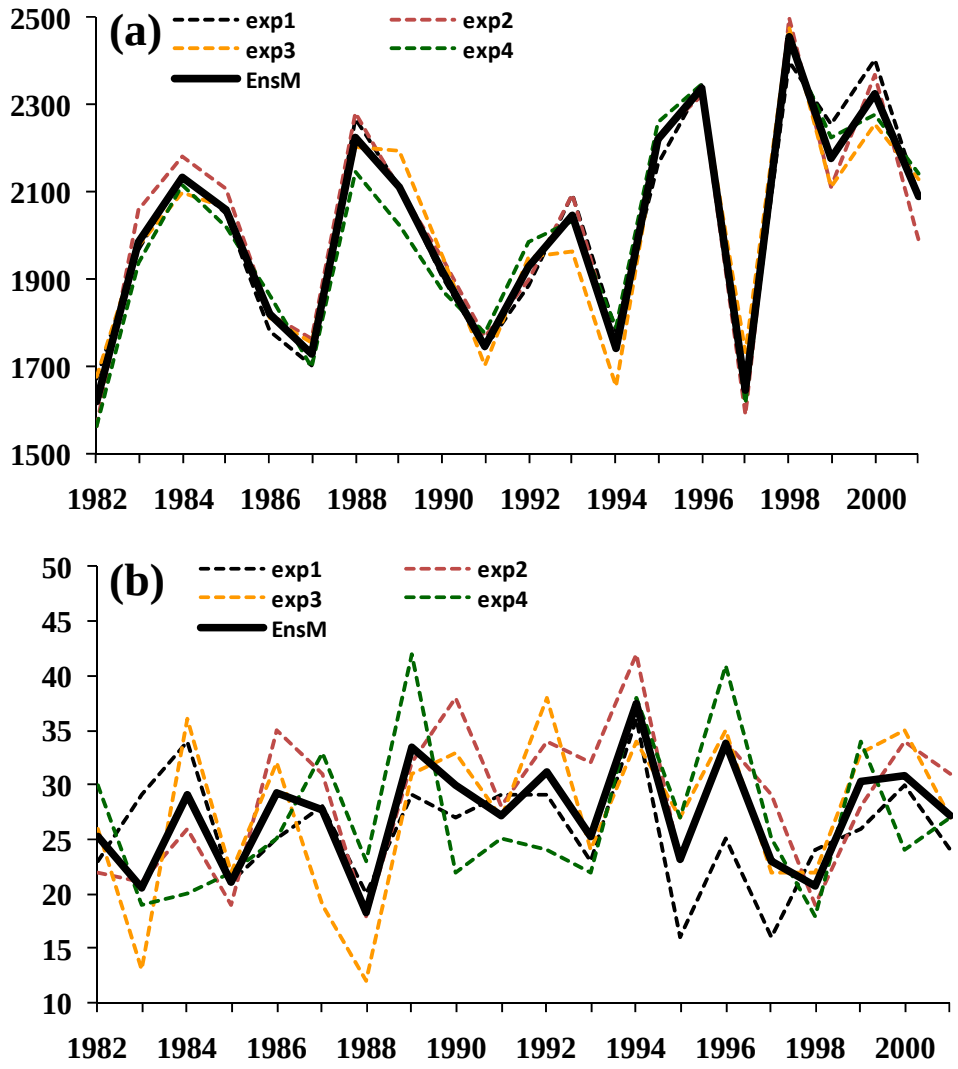

Figure 10. Numbers of TC-like vortices during the typhoon season in the four simulations and the ensemble mean: (a) Initial TC-like vortices without duration and intensity constraints; (b) TC-like vortices lasting not less than 2 days but without intensity constraint.

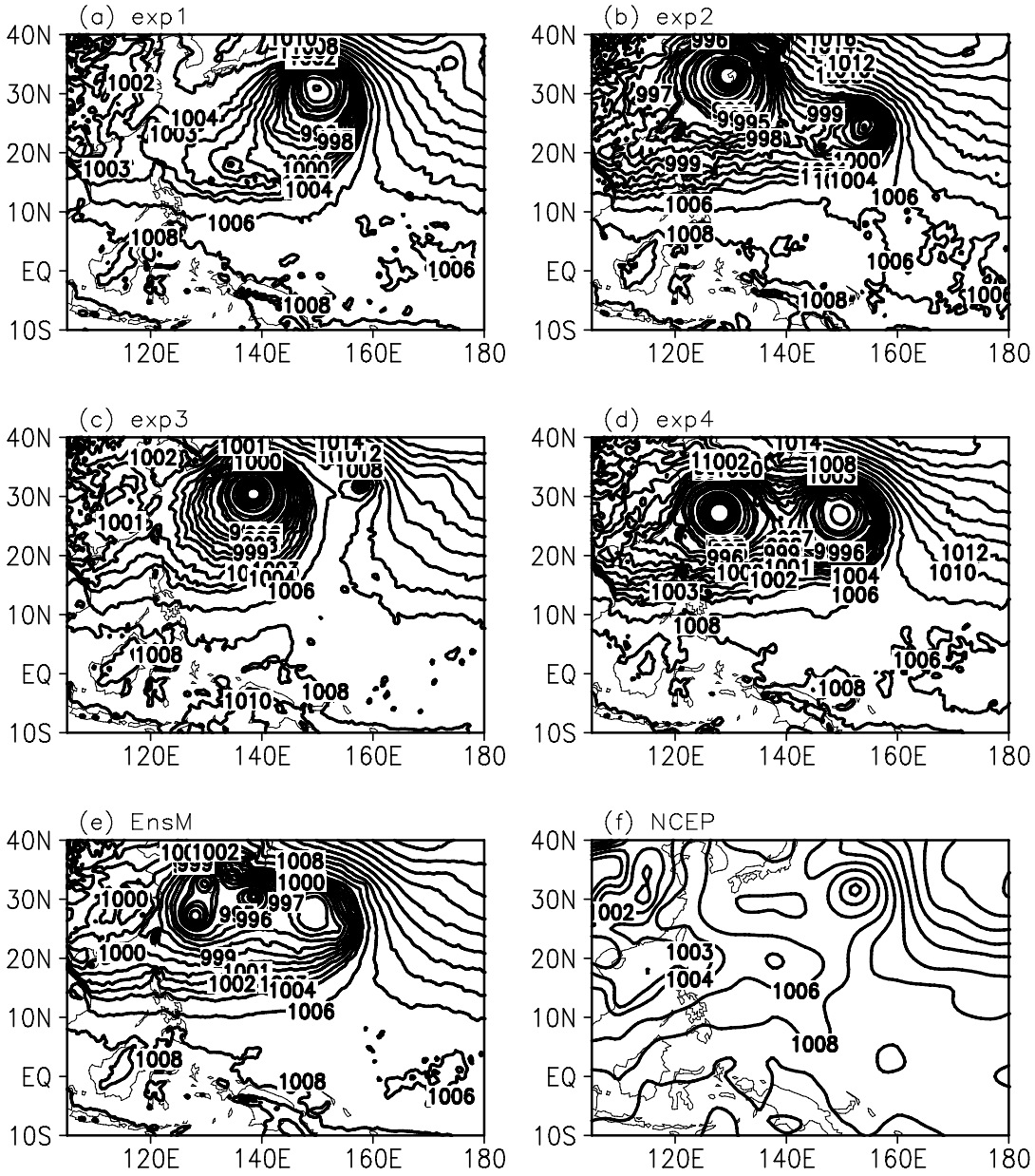

Figure 11. SLP fields at 12 UTC 26 July 1990 in the simulations and the NCEP reanalysis.

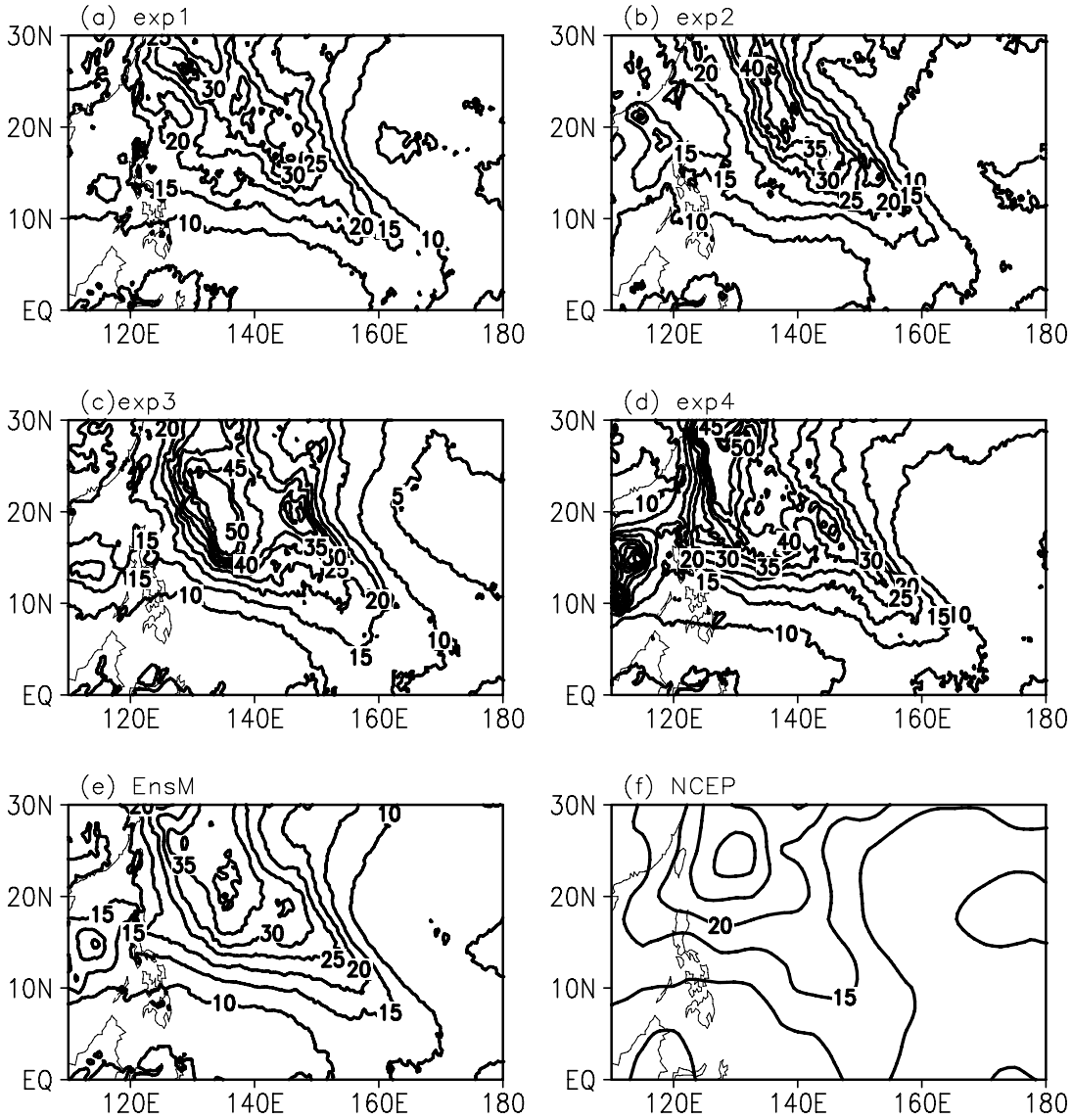

Figure 12. EKE at 850 hPa ($m^2 s^{-2}$) averaged in the typhoon season of 1990.

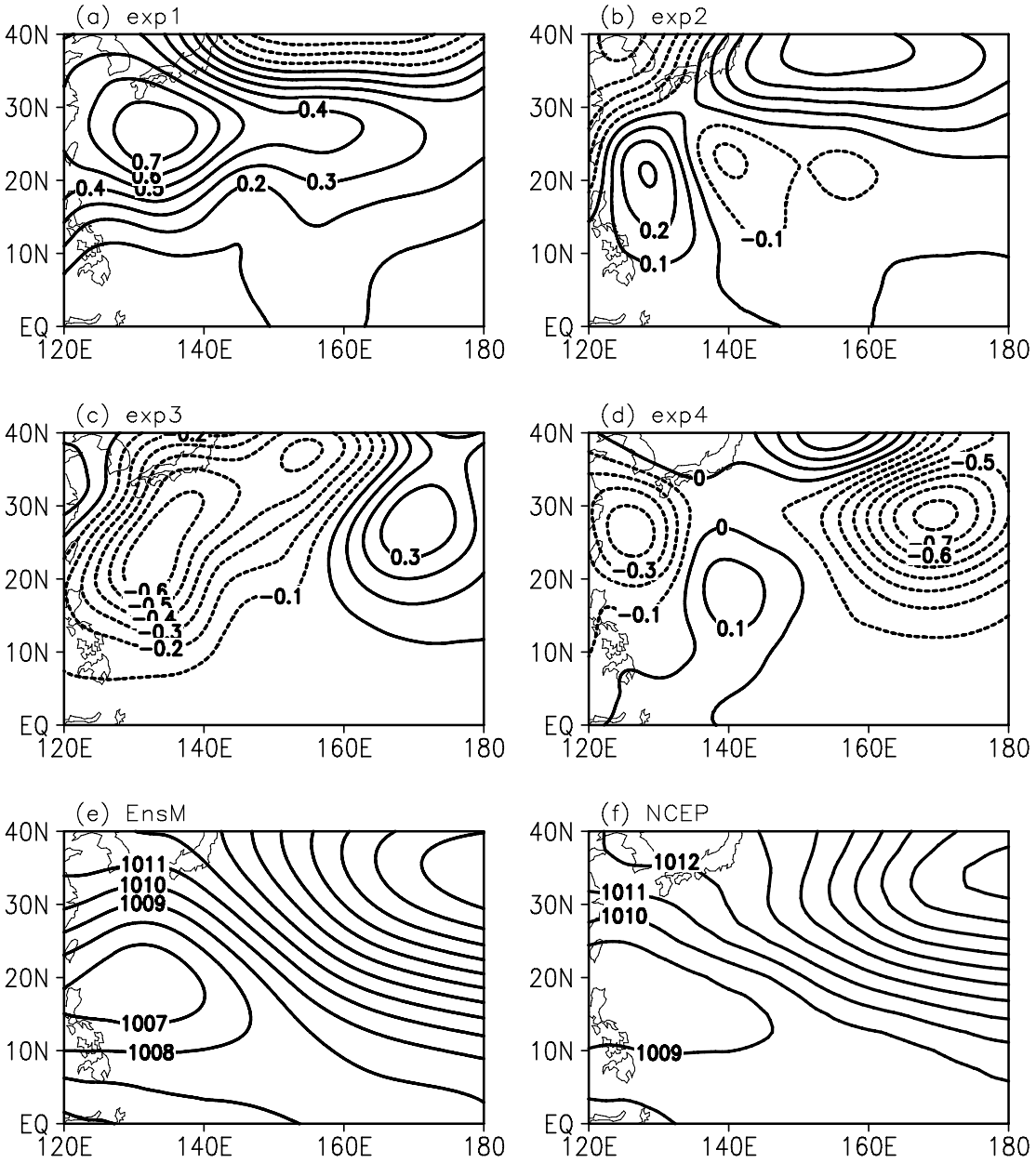

Figure 13. Filtered SLP anomalies from the ensemble mean in the four simulations, and filtered SLP in the ensemble mean and the NCEP reanalysis with wavelength longer than 1000 km averaged in the typhoon season of 1990.

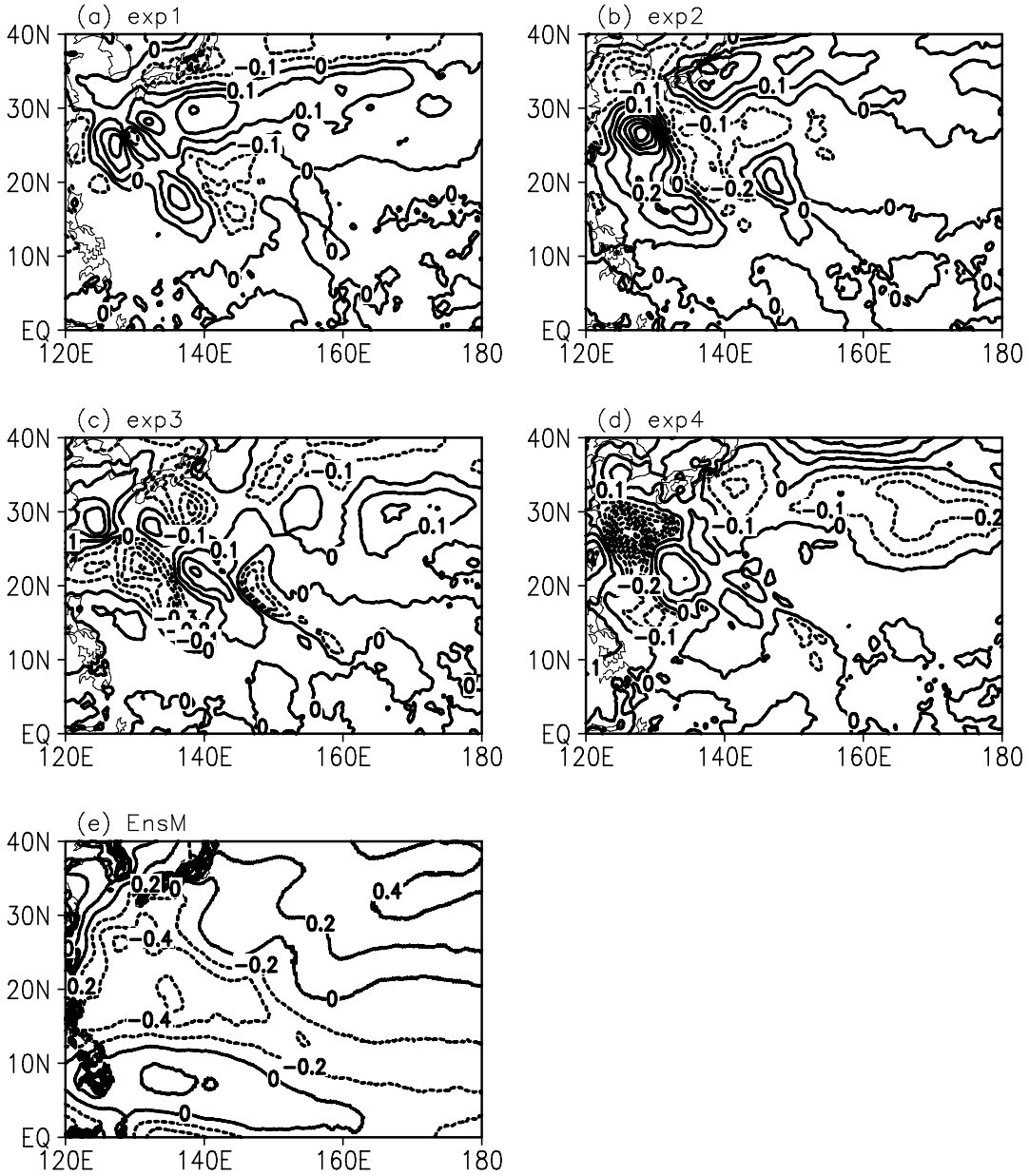

Figure 14. The same as in Figure 13, but for filtered SLP anomalies in all simulations and filtered SLP in the ensemble mean with wavelength shorter than 1000 km.

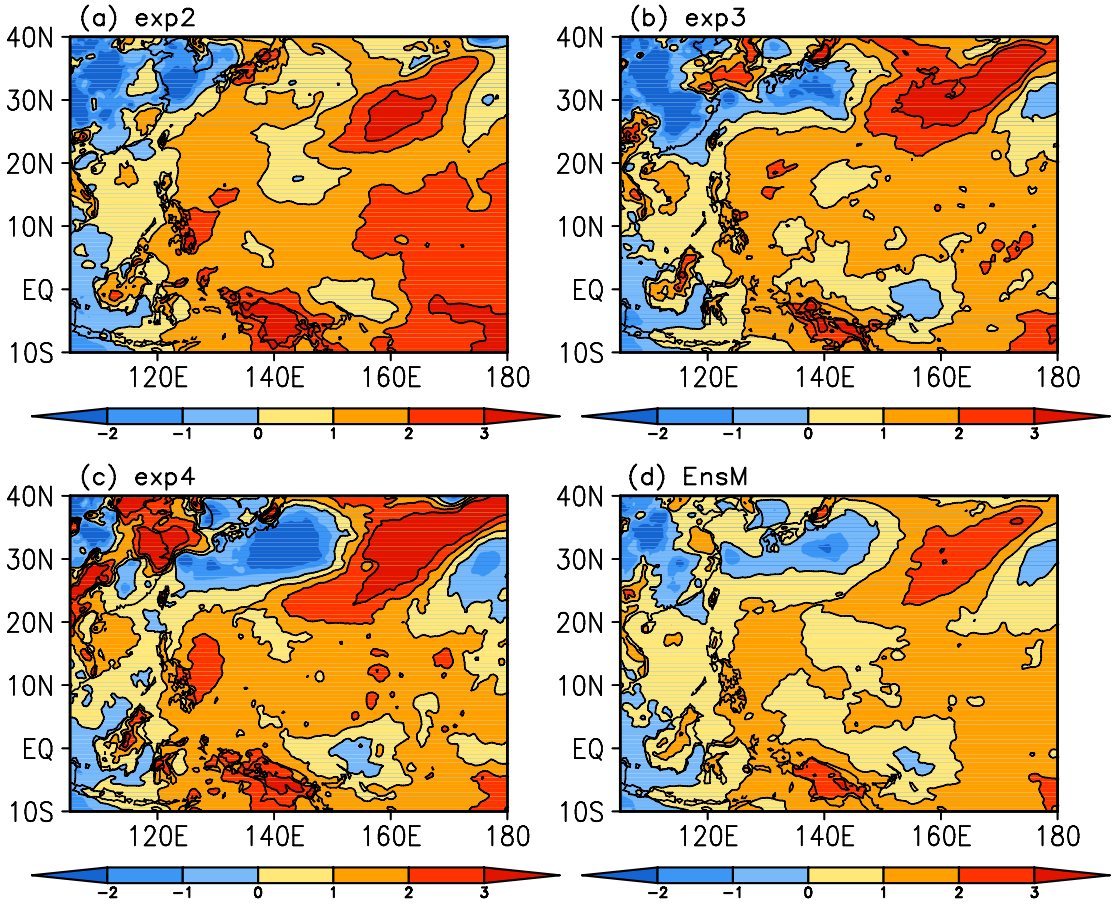

Figure 15. Differences in SLP fields between EXP1 and other simulations at 00 UTC 1 July 1990.

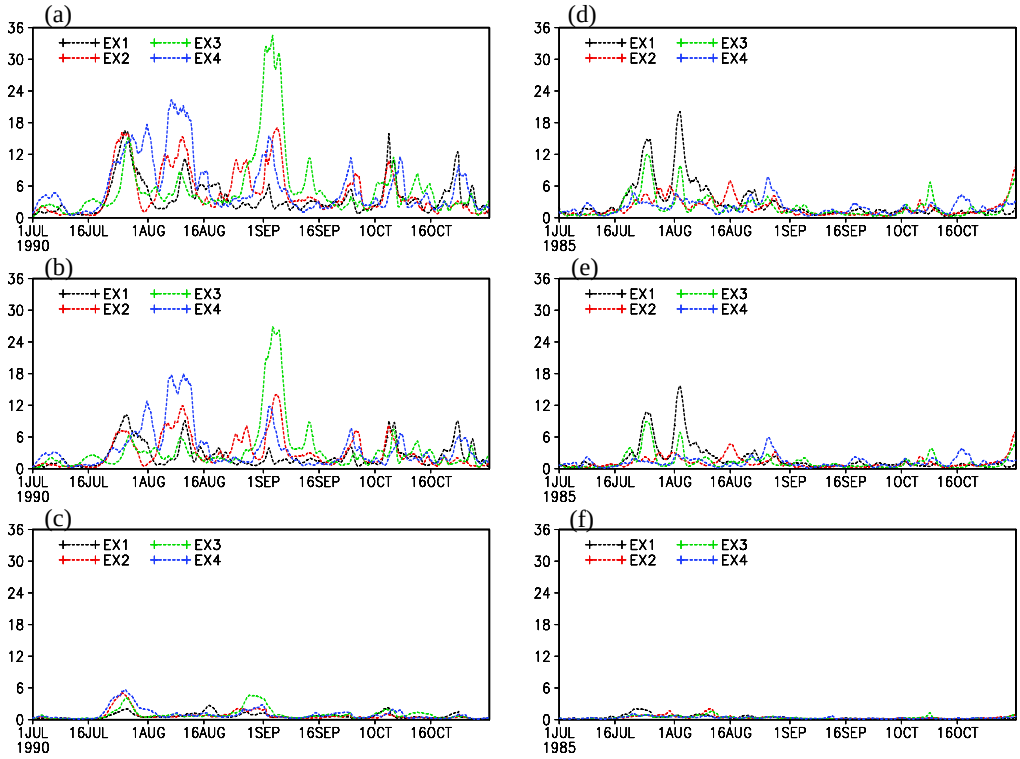

Figure 16. Domain-averaged variance in SLP (hPa) between the individual simulations and their ensemble mean for the largest variance year 1990 (left) and the smallest variance year 1985(right): unfiltered (top), large-scale with wavelength longer than 1000 km (middle), and small-scale with wavelength shorter than 1000 km (bottom).

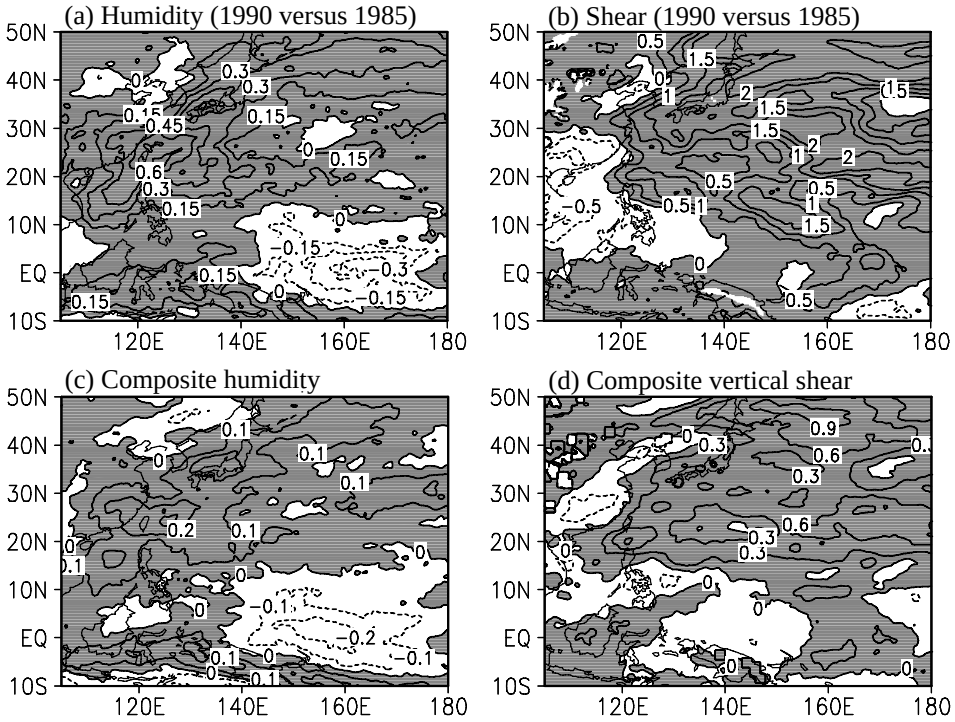

Figure 17. Differences in RMS fields of daily zonal wind vertical shear between 200 hPa and 850 hPa and 700 hPa specific humidity between year 1990 and year 1985 (a, b), and between the large variance and small variance years (c, d), see text for details.